Available online at www.sciencedirect.com
SCIENCE DIRECT®
Journal of Catalysis 221 (2003) 378–385
JOURNAL OF CATALYSIS
www.elsevier.com/locate/jcat

Characterizations and catalytic properties of fine particles of Ni–Sn intermetallic compounds supported on SiO_2

Ayumu Onda,* Takayuki Komatsu, and Tatsuaki Yashima

Department of Chemistry, Tokyo Institute of Technology, 2-12-1 Ookayama, Meguro-ku, Tokyo, Japan

Received 11 June 2003; revised 19 August 2003; accepted 20 August 2003

Abstract

Fine particles of Ni–Sn intermetallic compounds (IMCs) of Ni_3Sn, Ni_3Sn_2, and Ni_3Sn_4 with specific crystal structures were selectively prepared on SiO_2 by chemical vapor deposition (CVD) of $Sn(CH_3)_4$ onto Ni/SiO_2. X-ray photoelectron spectroscopy (XPS) and temperature-programmed reduction (TPR) measurements indicated that the near surface of these fine particles with atomic Ni/Sn ratios of 3/1, 3/2, and 3/4 are similar to those of corresponding unsupported Ni–Sn IMCs. X-ray diffraction (XRD) patterns of the fine particles showed peaks too broad to determine these crystal structures. Each unsupported Ni–Sn IMC was clarified to exhibit a specific Ni *K*-edge and Sn *K*-edge X-ray absorption near-edge structure (XANES) spectrum. The crystal structures of fine particles were by the identified by the fingerprinting method by Ni *K*-edge and Sn *K*-edge XANES spectra. Both these XANES spectra of Ni–Sn IMC/SiO_2 catalysts with Ni/Sn atomic ratios of 3/1, 3/2, and 3/4 were similar to those of unsupported Ni_3Sn, Ni_3Sn_2, and Ni_3Sn_4, respectively. The particles would have an average diameter of 3–4 nm obtained by TEM. Each Ni–Sn IMC particle showed intrinsic properties for the adsorption of carbon monoxide and hydrogen. The fine-particle catalysts exhibited high benzene selectivity (> 99% C) at high conversion for cyclohexane dehydrogenation. The selectivity was almost the same as that of the Ni–Sn IMC/SiO_2 catalysts with large particle sizes (about 15 nm), whose crystal structures were clearly determined by XRD, but was completely different from that of the Ni/SiO_2 catalyst. The activities of fine-particle catalysts were about 15 times higher than those of the large-particle catalysts.

Keywords: Ni–Sn; Intermetallic compounds; Fine particles; Absorptions of CO and H_2; Cyclohexane dehydrogenation

1. Introduction

Two kinds of metals in intermetallic compounds (IMCs) interact strongly with each other. This interaction includes a small contribution of a covalent bond. IMCs are expected to have unique catalytic properties because the surface atoms of IMCs have different electronic and geometric structures from those of pure metals. However, the catalytic properties of IMC itself have not been clarified satisfactorily. Most of the investigations on catalysis by IMC have dealt with so-called hydrogen-storage alloys [1–4] because of their unique activity for hydrogen dissociation and the possibility for the stored hydrogen to participate in the reactions. On the other hand, we have already reported unique catalytic selectivities of Co–Ge [5], Pt–Ge [6], and Ni–Sn [7] IMCs, which are not hydrogen-storage alloys. The surface of these compounds is composed of metallic atoms after reduction treatment. The IMC catalysts containing Co or Ni show much lower activity than pure Co or Ni for H_2–D_2 equilibration but give high selectivity to ethylene in the hydrogenation of acetylene. Pt–Ge IMCs show high selectivity to butene in the hydrogenation of 1,3-butadiene. Pd_3Pb catalysts show high selectivity to methyl methacrylate for the oxidative esterification of methacrolein and methanol [8]. These IMC catalysts show lower activities than their component monometallic catalysts, such as pure Pt catalyst. In contrast, Pt_3Ti catalysts show higher activity than those of pure Pt catalysts for H_2–D_2 equilibration and ethylene hydrogenation [9]. However, the activities of the above-noted IMC catalysts, except for Pd_3Pb, suffer from low specific surface areas because they are prepared by melting the mixture of two component metals at higher temperatures than their melting points and crushing the ingots of IMC. The diameters of these unsupported IMC powder are about 30 μm.

* Corresponding author: Research Laboratory of Hydrothermal Chemistry, Faculty of Science, Kochi University, Akebono-cho 2-5-1, Kochi 780-8520, Japan.
E-mail address: onda@cc.kochi-u.ac.jp (A. Onda).

0021-9517/$ – see front matter
doi:10.1016/j.jcat.2003.08.012

To improve specific surface areas and catalytic activities of IMC catalysts, recently we tried to prepare the particles of single-phase IMC on supports, such as SiO_2 and zeolites. It was reported that chemical vapor deposition (CVD) of organometallic compounds, e.g., $Sn(n\text{-}C_4H_9)_4$, occurs selectively onto novel metals, such as Rh and Pt, supported on SiO_2 [10–13]. In a previous study, we reported on the selective preparation of particles of single-phase Ni_3Sn, Ni_3Sn_2, and Ni_3Sn_4 on SiO_2 by CVD of $Sn(CH_3)_4$ onto Ni/SiO_2 and thermal treatments [14,15]. The diameters of Ni–Sn IMC particles on SiO_2 are about 15 nm. The supported IMC catalysts show almost the same selectivity for the acetylene hydrogenation and for cyclohexane dehydrogenation as the corresponding unsupported IMC catalysts, and show about 1000 times higher activities than those of unsupported ones. This high activity is due to the enhancement of dispersion of IMCs. However, the activities of the supported catalysts are not satisfactory. The fine particles of IMC are expected to have not only high catalytic activity but also significantly different catalytic properties from the unsupported IMC by the particle-size effect. For supported Au and Pt monometallic catalysts, the catalytic properties depend on their particle sizes between 1 and 3 nm [16–18]. However, the determination of IMC species is hard for fine particles. A particle size of about 10 nm is needed to clearly determine three kinds of Ni–Sn IMC structures by powder X-ray diffraction (XRD) in previous work [14,15].

In this study, we will analyze bulk structures of the Ni–Sn fine particles on SiO_2 by X-ray absorption fine structure (XAFS) measurement, which is a useful measurement for structures of clusters and fine particles [19–21]. The analysis of IMC structure by XAFS is expected to solve the problem of identifying ultrafine IMC species. In addition, IMC fine particles will be characterized by X-ray photoelectron spectroscopy (XPS) and temperature-programmed reduction (TPR) measurements and used as catalysts for the dehydrogenation of cyclohexane. Their catalytic activity and selectivity will be compared with those of three kinds of SiO_2-supported large IMC particle (about 15 nm) catalysts, which have a single phase of Ni_3Sn, Ni_3Sn_2, and Ni_3Sn_4 determined by XRD.

2. Experimental methods

2.1. Preparation of catalysts

Two kinds of Ni/SiO_2 were prepared by ion-exchange (Ni/SiO_2A; 4 wt% Ni) and incipient wetness (Ni/SiO_2C; 5 wt% Ni) methods. The preparation method of Ni/SiO_2A with small nickel particles was as follows. Silica, SiO_2A (Deggusa, Aerosil 200) was soaked in an aqueous solution of ammonia (0.2 wt% NH_3) to exchange the surface protons with ammonium ions for 0.5 h at room temperature and filtered off. $Ni(NO_3)_2 \cdot 6H_2O$ was dissolved in an aqueous solution of ammonia (0.2 wt% NH_3) to form a $[Ni(NH_3)_6]^{2+}$ complex. The ammonium-exchanged silica was soaked in the solution of $[Ni(NH_3)_6]^{2+}$ for 1 h at room temperature. Then the solid was filtered off, dried at 343 K for 12 h in air, heated to 723 K (5 K min^{-1}) with flowing hydrogen (100 ml min^{-1}), and kept at 723 K for 1 h. Ni/SiO_2A thus prepared was cooled with flowing hydrogen to room temperature and stored in air. The preparation method of Ni/SiO_2C with large nickel particles was as follows. Silica gel, SiO_2C (Fuji-Silysia, Cariact G-6), was impregnated in an aqueous solution of $Ni(NO_3)_2$ by the incipient wetness method. Then the solid was dried at 400 K for 8 h, calcined at 723 K for 4 h in air, and reduced with flowing hydrogen (100 ml min^{-1}) at 723 K for 4 h. Ni/SiO_2C thus prepared was cooled with flowing hydrogen to room temperature and stored in air.

Silica-supported Ni–Sn IMCs were prepared by the following method. After the stored Ni/SiO_2A or Ni/SiO_2C was again reduced in a fixed-bed reactor under atmospheric pressure at 723 K with flowing hydrogen, CVD of $Sn(CH_3)_4$ (Soekawa Chemicals) was carried out [14,15]. The vapor of $Sn(CH_3)_4$ (4 kPa) was introduced onto Ni/SiO_2A or Ni/SiO_2C at 343–523 K with H_2 as carrier gas (30 ml min^{-1}). After the CVD treatment, the temperature at the sample bed was raised to 623–1173 K and kept at the same temperature for 1 h in flowing hydrogen (100 ml min^{-1}). The sample was cooled with flowing hydrogen into room temperature and stored in air.

Unsupported Ni–Sn IMCs, Ni_3Sn, Ni_3Sn_2, and Ni_3Sn_4 were prepared by melting the mixture of nickel (Koch Chemicals, 99.99%) and tin (Soekawa Chemicals, 99.99%) powders with an SiC electric furnace in flowing argon [7]. The temperature was raised by 5 K min^{-1} to 1733 K to melt the mixture and kept at 1733 K for 1 h. To anneal the samples, the temperature was lowered to 1120 K (Ni_3Sn), 1210 K (Ni_3Sn_2), and 740 K (Ni_3Sn_4), which are lower by 50 K than the melting temperatures of Ni_3Sn, Ni_3Sn_2, and Ni_3Sn_4 [22], respectively, and kept at these temperatures for 8 h in flowing argon. The samples were cooled with flowing argon to room temperature and stored in air. The resultant ingots were crushed in air and filtered into the powder with diameters of 25–38 μm. The powder of pure nickel (Koch Chemicals, 99.99%) was also filtered to have diameters of 25–38 μm.

2.2. Characterization methods

The samples were dissolved with the aqua regia, and then the compositions of samples were determined by ICP (Rigaku, JY38). The crystal structure of samples was analyzed by powder X-ray diffraction (Rigaku, RINT2400). The X-ray source was Cu-K_α at 40 kV and 100 mA.

Chemisorption measurements of carbon monoxide and hydrogen on supported catalyst powders (0.10 g) were taken at room temperature in a glass closed system. Before the chemisorption studies, each catalyst was reduced with flowing hydrogen (100 ml min^{-1}) at 773 K for 1 h. Transmission infrared spectra of pressed disks of catalysts (5 mg cm^{-2}) at room temperature were recorded at 4 cm^{-1} resolution with

a FT/IR 430 (Jasco). Before the measurement, each catalyst was set in a quartz cell with CaF_2 windows and reduced with flowing hydrogen (100 ml min^{-1}) at 773 K for 1 h. CO gas of 1 kPa was introduced into the cell and vacuumed from the cell at room temperature.

XPS spectra of supported and unsupported IMCs or the component pure metals were obtained by using Escalab 220i (Fisons Inst.) with an X-ray source of Al-K_α. The sample pressed into a pellet was put in a pretreatment chamber. Before and after a reduction treatment with flowing hydrogen (101 kPa) at 773 K for 1 h, the sample was transferred into the spectrometer in vacuo (under 10^{-7} Pa) to measure the spectra. Binding energies were obtained using C 1s peak (284.5 eV) as a standard.

The reduction behavior of the catalysts stored in air was examined by temperature-programmed reduction. Under flowing H_2(5%)/N_2, the temperature of the sample bed was raised from room temperature to 873 K at a heating rate of 10 K min^{-1} and the consumption of hydrogen was continuously measured by a TCD detector. Trace amounts of oxygen and water in the H_2/N_2 gas and water produced by the reduction of samples were removed by passing through columns of OMI-1 (Spelco) and P_2O_5 (Soekawa Chemicals).

The Ni *K*-edge and Sn *K*-edge XANES spectra were measured at BL-10B [23] of the Photon Factory at the Institute Material Structure Science, High Energy Accelerator Research Organization (KEK-IMSS-PF), in a transmission mode at room temperature. The storage ring was operated at an electron energy of 2.5 GeV and stored current of 320–400 mA. The synchrotron radiation was monochromatized by a Si (311) channel-cut monochromator at BL-10B. Normalization of XANES was carried out as described elsewhere [24]. The wafers of supported catalysts were reduced with flowing hydrogen (100 ml min^{-1}) at 773 K for 1 h and enclosed into a doubled polyethylene pack with Mn/SiO_2 and silica gel in a glove box under pure argon gas, whereas no treatment for the wafers of unsupported catalysts was carried out.

2.3. Catalytic properties

After the stored catalysts were reduced in a fixed-bed flow reactor under atmospheric pressure at 773 K with flowing hydrogen (100 ml min^{-1}) for 1 h, the dehydrogenation of cyclohexane was carried out. Cyclohexane (Wako Pure Chemical Ind. 99.8%) was previously dehydrated with 5A molecular sieves (Wako Pure Chemical Ind.). The vapor of cyclohexane (3.7 kPa) was introduced into the reactor at 673 K with hydrogen as a carrier gas (30–100 ml min^{-1}). The amount of supported catalysts was 0.050 g. The composition of gaseous hydrocarbons was monitored with FID gas chromatography (Shimadzu GC 8A).

3. Results and discussion

3.1. Preparation and characterization

3.1.1. Preparation of silica-supported Ni–Sn intermetallic compound fine particles

Chemical vapor deposition of $Sn(CH_3)_4$ onto reduced Ni/SiO_2A and subsequent hydrogen treatments at high temperature were carried out for the preparation of fine particles of single-phase Ni_3Sn, Ni_3Sn_2, and Ni_3Sn_4. The Ni/SiO_2A was prepared by the ion-exchange method and the nickel content was 4 wt% determined by ICP chemical analysis. The amount of deposited tin atoms increased with increasing CVD temperature and was controlled by the CVD temperature. CVD at 365, 413, and 460 K for 1 h onto Ni/SiO_2A resulted in Ni/Sn atomic ratios determined by ICP that were 3/1.05, 3/2.13, and 3/4.04, respectively. These ratios were close to stoichiometric compositions of Ni_3Sn, Ni_3Sn_2, and Ni_3Sn_4 and the deviations were within the composition widths in phase diagrams [22] and were almost equal to the error of ICP measurements. Whereas in the case of Ni/SiO_2C [15], CVD at 423, 448, and 498 K for 1 h resulted in Ni/Sn ratios close to each stoichiometric composition. The temperature of CVD to obtain specific Ni/Sn ratios depended on the nickel particle sizes of the parent Ni/SiO_2. The average diameters of nickel particles in Ni/SiO_2A and Ni/SiO_2C were about 3 and 8 nm, respectively, which were estimated by the chemisorption measurement of H_2.

After CVD, the Ni–Sn bimetallic particles on SiO_2A were heated to form each single phase of IMC structure under flowing hydrogen at 773 K. The structure of Ni–Sn fine particles on SiO_2A was analyzed by powder X-ray diffraction. As shown in Fig. 1, diffraction peaks appeared around 30 and 43° of 2θ and grew with increasing Sn content. These peaks suggested the formation of Ni–Sn IMC phases. However, the peaks were too broad to determine the kind of Ni–

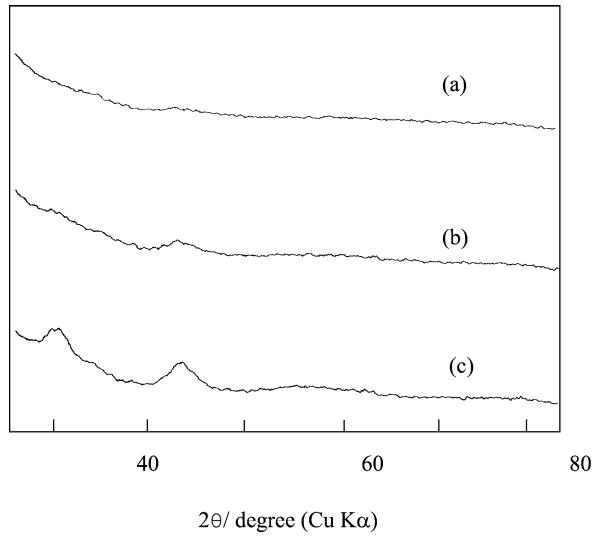

Fig. 1. XRD patterns of Ni_3Sn/SiO_2A (a), Ni_3Sn_2/SiO_2A (b), and Ni_3Sn_4/SiO_2A (c).

Table 1
The average diameters of particles on SiO_2A and the amount of adsorbed CO and H_2 at room temperature

Fine particles on SiO_2A	Average diameter[a] (nm)	Amount of adsorption (10^{-5} mol g_{cat}^{-1})	
		CO	H_2
Ni_3Sn	3	10	0.6
Ni_3Sn_2	3.5	9	0.03
Ni_3Sn_4	4	3	0.00
Ni	3[b]	13	8
Sn	n.d.	0.00	0.00

n.d., not detected.
[a] Average diameters were estimated by TEM.
[b] An average diameter was calculated by the amount of adsorption of hydrogen.

Sn IMCs, which have some peaks around 30 and 43° of 2θ in XRD patterns. The average diameters of the fine Ni–Sn particles on SiO_2A were estimated by TEM and summarized in Table 1. The TEM images are shown in Fig. 2. The average diameters were about 3–4 nm and increased with increasing Sn content in Ni–Sn IMC/SiO_2A. In this study, no particle was observed in the TEM image of Ni/SiO_2A, which may be due to the oxidization of small metallic Ni particles into unobvious species in air.

Fig. 3 shows infrared spectra of adsorbed CO on Ni/SiO_2A and three kinds of Ni–Sn IMC/SiO_2A. CO molecules were adsorbed in a linear type on all Ni–Sn IMC/SiO_2A samples. In contrast, on Ni/SiO_2A CO molecules were adsorbed not only in a linear type but also in a bridge type. The infrared spectra indicated that most of the nickel particles interacted with tin atoms after CVD of $Sn(CH_3)_4$ onto Ni/SiO_2A.

The amounts of CO adsorbed on the catalysts, as shown in Table 1, decreased with increasing Sn contents in Ni–Sn IMC/SiO_2A samples. The amounts were comparable to amounts of surface nickel atoms, which were roughly estimated from total Ni/Sn ratios, average particle diameters, and the ratios of linear to bridge types in IR spectra of CO adsorption. Therefore, the CO adsorption measurements supported the average diameters of Ni–Sn and Ni fine particles estimated by TEM and H_2 adsorption measurements. However, the amounts of adsorbed H_2 on Ni–Sn IMC/SiO_2A samples were very small and much decreased with decreasing Ni/Sn ratios as shown in Table 1. The adsorption measurements of CO and H_2 clarified that the surface of each Ni–Sn particles with total Ni/Sn ratios of 3/1, 3/2, and 3/4 shows a specific adsorption property. XRD patterns and infrared spectra suggested that an Ni–Sn IMC phase formed in the bulk and surface of Ni–Sn particles on SiO_2A.

3.1.2. Temperature-programmed reduction

In a previous study, we carried out TPR measurements for supported (SiO_2C) and unsupported Ni_3Sn, Ni_3Sn_2, and Ni_3Sn_4, which were determined clearly by XRD, together with pure Ni and pure Sn after storage in air [15]. The unsupported Ni and Ni–Sn IMCs show each specific TPR profile.

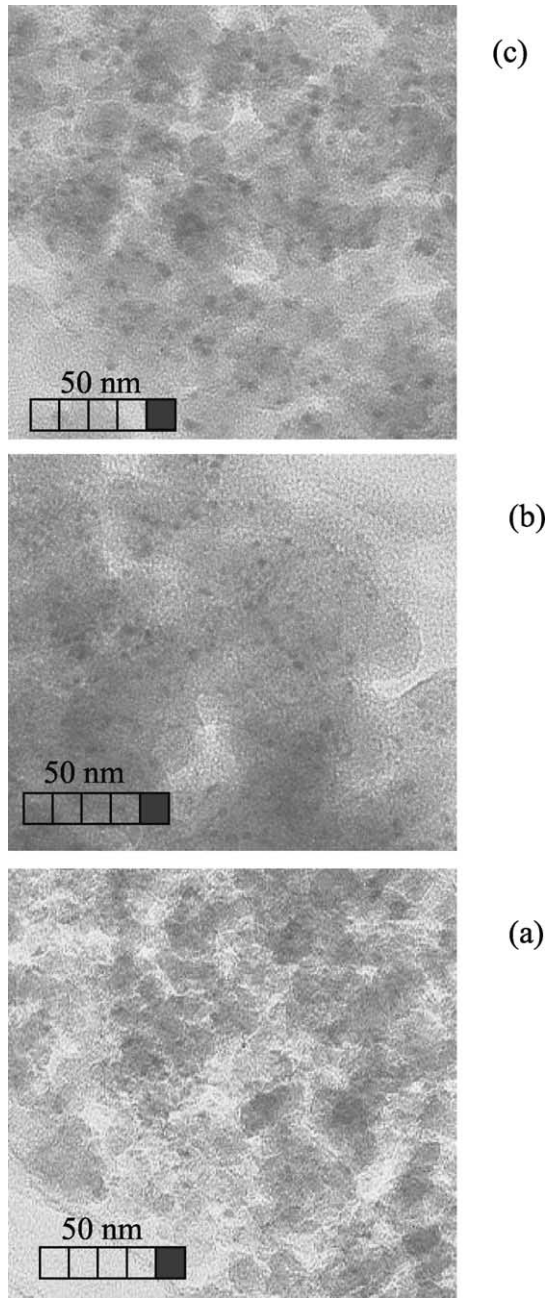

Fig. 2. TEM images of Ni_3Sn/SiO_2A (a), Ni_3Sn_2/SiO_2A (b), and Ni_3Sn_4/SiO_2A (c).

The Ni–Sn IMC/SiO_2C shows almost the same reduction behavior as that of the corresponding unsupported Ni–Sn IMCs. Therefore, TPR is a useful method for determining what kind of Ni–Sn IMC is present on the surface. Next, we tried to determine the Ni–Sn IMC species supported on SiO_2A by TPR.

In a previous study, TPR measurements were carried out without pretreatment of samples. However, all TPR profiles of Ni–Sn IMC/SiO_2A samples without pretreatment showed broad peaks at around 600 K, which were larger than peaks of Ni_3Sn_4/SiO_2A around 600 K in Fig. 4. The large peaks indicated that Ni–Sn fine particles might be deeply oxidized

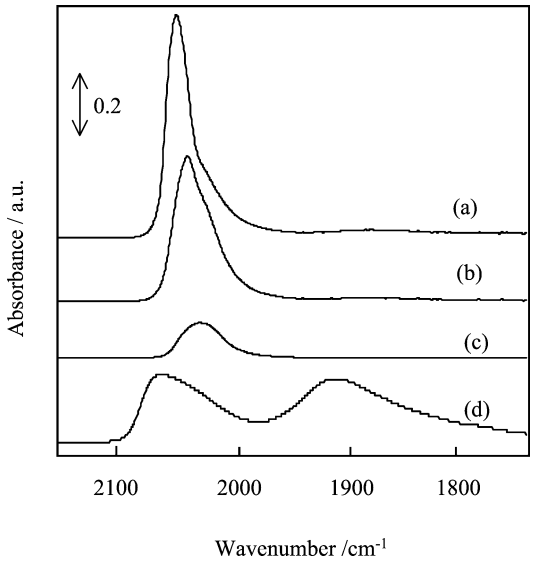

Fig. 3. IR spectra of CO adsorbed on Ni_3Sn/SiO_2A (a), Ni_3Sn_2/SiO_2A (b), Ni_3Sn_4/SiO_2A (c), and Ni/SiO_2A (d) after reduction with flowing hydrogen at 773 K for 1 h.

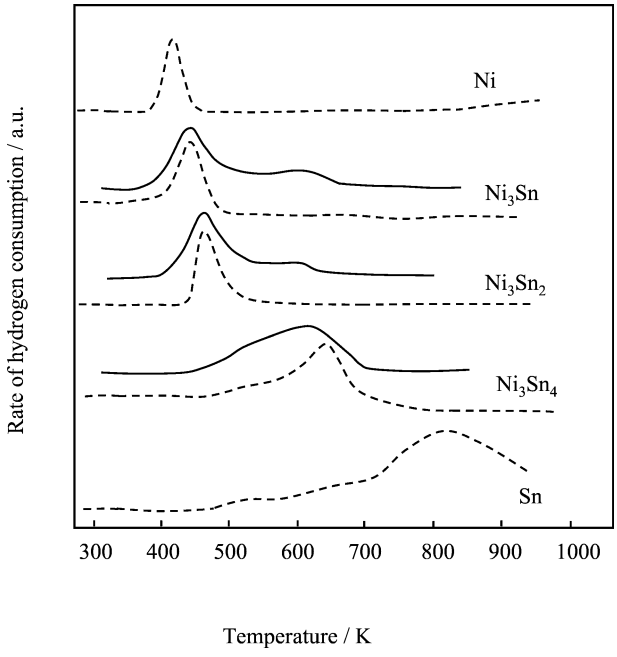

Fig. 4. TPR profiles of Ni–Sn IMC fine particles supported on SiO_2A (solid lines) and Ni–Sn IMC, Ni, and Sn large particles supported on SiO_2C (broken lines).

in air at room temperature and strongly interact with SiO_2. Therefore, in this study, Ni–Sn IMC/SiO_2A samples were pretreated with hydrogen at 773 K for 0.5 h in order to reduce fine particles and subsequently with air of 3 pulses of 1 ml at room temperature in order to air-oxidize only outside of the fine particles.

Fig. 4 shows the TPR profiles of Ni_3Sn/SiO_2A, Ni_3Sn_2/SiO_2A, and Ni_3Sn_4/SiO_2A after the pretreatment, together with those of Ni, Sn, and Ni–Sn IMCs supported on SiO_2C. Ni_3Sn/SiO_2A and Ni_3Sn_2/SiO_2A had one peak at 441 and 472 K, respectively. Ni_3Sn_4/SiO_2A had two peaks at about 540 and 610 K. In Ni–Sn IMC/SiO_2C, Ni_3Sn and Ni_3Sn_2 had one peak at 448 and 468 K, respectively. Tin oxides (Sn^{4+}) in air-oxidized Ni_3Sn and Ni_3Sn_2 would be reduced at almost the same temperature as nickel oxides [7]. Ni_3Sn_4 had two peaks at 523 and 653 K. Though the TPR peaks of Ni–Sn IMC/SiO_2A samples were broader than those of Ni–Sn IMC/SiO_2C samples, they appeared at almost the same temperature as those of corresponding Ni–Sn IMC/SiO_2C. The results indicate that fine particles of each Ni–Sn IMC are formed on SiO_2A. At around 600 K, all Ni–Sn IMC/SiO_2A showed a broad peak, which did not appear in the profiles of Ni–Sn/SiO_2C. Though this peak could indicate the coexistence of Ni_3Sn_4 species, this peak would probably be from the above-described Ni–Sn fine particles oxidized by pulsed air and strongly interacting with SiO_2.

Table 2
XPS data of Ni–Sn IMC/SiO_2A

Sample	Binding energy (eV)		Ni/	Ni/(Ni+Sn)×100	
	Ni $2p_{3/2}$	Sn $3d_{5/2}$	(Ni+Sn) ×100	Unsupported IMC[a]	SiO_2C[b]
Ni_3Sn/SiO_2A	852.4	485.0	56	57	56
Ni_3Sn_2/SiO_2A	852.3	485.1	45	48	42
Ni_3Sn_4/SiO_2A	852.4	485.2	20	28	22

[a] Values of unsupported Ni–Sn IMC.
[b] Values of Ni–Sn IMC supported on SiO_2C [15].

3.1.3. X-ray photoelectron spectroscopy

Table 2 shows XPS data for the Ni–Sn IMC/SiO_2A after reduction with flowing hydrogen at 773 K for 1 h. The binding energies of Ni $2p_{3/2}$ (852.3–852.4 eV) and Sn $3d_{5/2}$ (485.0–485.2 eV) clarified the reduction of surface Ni and Sn atoms to Ni^0 and Sn^0 in all Ni–Sn IMC/SiO_2A. The binding energies seemed to shift slightly from those of metallic Ni (852.7 eV) and Sn (485.0 eV) [7,25], respectively. However, the shifts did not have a clear relation with Ni/Sn ratios, which was similar to the case of unsupported Ni–Sn IMCs [7]. We measured the binding energy of Ni 3d near the Fermi level for unsupported Ni–Sn IMCs [7]. The Ni 3d peaks shifted regularly with Ni/Sn ratios toward high binding energy, and these shifts indicate the increase and localization of electron density in Ni 3d orbitals with increasing Sn contents. However, the XPS spectra near the Fermi level for the Ni–Sn IMC/SiO_2A were not observed clearly in this study.

The proportions of nickel atoms near the surface of Ni–Sn fine particles on SiO_2A are shown in Table 2 as Ni/(Ni + Sn) atomic ratios determined from the peak areas of Ni $2p_{3/2}$ and Sn $3d_{5/2}$ XPS spectra. The actual proportion may be higher than the values in Table 2, because it is difficult to integrate completely the peak areas of Ni $2p_{3/2}$ containing many satellite peaks [26]. The Ni/(Ni + Sn) values of Ni_3Sn/SiO_2A, Ni_3Sn_2/SiO_2A, and Ni_3Sn_4/SiO_2A were 56, 45, and 20%, respectively, which were almost the same as those of Ni_3Sn,

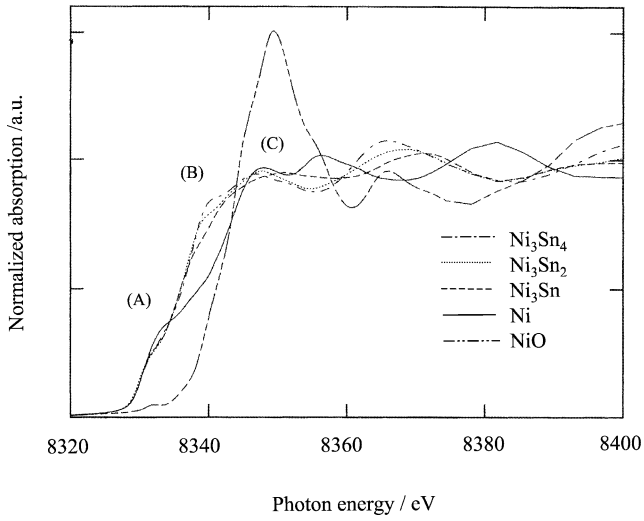

Fig. 5. Ni K-edge XANES spectra of Ni foil and unsupported NiO and Ni–Sn IMCs.

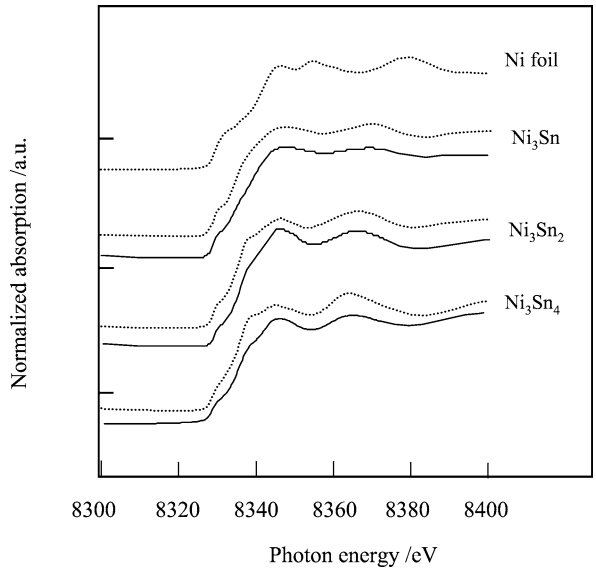

Fig. 6. Ni K-edge XANES spectra of Ni–Sn IMC fine particles supported on SiO_2A (solid lines) and unsupported Ni–Sn IMCs (broken lines).

Ni_3Sn_2, and Ni_3Sn_4 unsupported and supported on SiO_2C, respectively [15].

The chemisorption, TPR, and XPS measurements show that Ni_3Sn/SiO_2A, Ni_3Sn_2/SiO_2A, and Ni_3Sn_4/SiO_2A had an intrinsic surface which was very similar to that of the corresponding unsupported IMCs and Ni–Sn IMCs supported on SiO_2C.

3.1.4. Fingerprinting identification by X-ray absorption near-edge structure (XANES)

As shown in Fig. 1, bulk structures of the Ni–Sn fine particles on SiO_2A could not be identified by XRD because the particles were too small. On the other hand, from TPR and XPS studies, the near surface of Ni–Sn fine particles was seen to have a similar nature to the corresponding Ni–Sn IMCs. However, the particles might have an egg-shell-type structure whose internal structure is different from the surface structure. Therefore, the structure analysis of Ni–Sn IMC/SiO_2A was carried out by Ni K-edge and Sn K-edge XANES measurements.

First, we measured the Ni K-edge XANES spectra of unsupported Ni_3Sn, Ni_3Sn_2, Ni_3Sn_4, Ni foil, and NiO (Fig. 5). A shoulder peak (A) appeared at 8334 eV for Ni foil and at 8332 eV for IMCs. The first inflection points of Ni–Sn IMCs were observed at almost the same photon energy of about 8328 eV as that of the Ni foil, which showed that Ni atoms in Ni–Sn IMCs were Ni^0. In the spectra of IMCs, a new absorption peak (B) appeared at about 8340 eV, whereas no peak appeared for the Ni foil. The intensity of peak (B) increased with decreasing Ni/Sn ratios, that is, $Ni < Ni_3Sn < Ni_3Sn_2 < Ni_3Sn_4$. The peak energy of the third peak (C) around 8347 eV for IMCs decreased with decreasing Ni/Sn ratios. It is clarified that three kinds of Ni–Sn IMCs exhibit each characteristic Ni K-edge XANES. In the case of Ni–Al IMC, Ni K-edge XANES spectra for Ni_3Al [27] are also different from those of pure Ni. Similar results were reported for Au–V [28] and Pd–Ti [29] systems. In conclusion, Ni K-edge XANES analysis is an effective method for the identification of Ni–Sn IMCs by the fingerprinting method.

Next, we measured the Ni K-edge XANES spectra of Ni_3Sn/SiO_2A, Ni_3Sn_2/SiO_2A, and Ni_3Sn_4/SiO_2A. Fig. 6 shows the normalized XANES spectra of Ni–Sn IMC/SiO_2A catalysts together with the spectra of unsupported Ni_3Sn, Ni_3Sn_2, and Ni_3Sn_4. The absorption peaks in spectra of Ni–Sn IMC/SiO_2A appeared at almost the same energy as those of the corresponding unsupported IMCs. The intensities of shoulder prepeaks at about 8330 eV of Ni–Sn IMC/SiO_2A samples were also almost the same as those of the unsupported ones. The bulk structures of the Ni–Sn fine particles on SiO_2A are similar to the corresponding unsupported Ni–Sn IMCs, whereas the absorption intensities at about 8340 eV in the spectra of Ni–Sn IMC/SiO_2A increased with decreasing tin content as well as those of unsupported IMCs, but were lower than those of unsupported IMCs. The peaks at about 8340 eV may depend on a particle size effect or a support effect.

Fig. 7 shows the normalized Sn K-edge XANES spectra of thee kinds of Ni–Sn IMC/SiO_2A catalysts and those of unsupported Ni_3Sn, Ni_3Sn_2, and Ni_3Sn_4. In Fig. 7, the Sn K-edge XANES spectra are overlapped for each preparation method in order to clarify the difference of each spectrum. The spectra of unsupported IMCs and Ni–Sn IMC/SiO_2A exhibited absorption peaks appeared around 29190–29200 eV and did not include a remarkable shoulder peak. According to the spectra of unsupported series, the order of normalized absorption intensities is $Ni_3Sn_4 > Ni_3Sn_2 > Ni_3Sn$ around 29190 eV and is $Ni_3Sn > Ni_3Sn_2 > Ni_3Sn_4$ around 29197 eV. The spectra of Ni–Sn IMC/SiO_2A catalysts are more similar to those of the corresponding unsupported Ni_3Sn, Ni_3Sn_2, and Ni_3Sn_4, except for the spectrum of Ni/Sn = 3/1 around 29197 eV. The order of normalized absorption intensities around 29190 and 29197 eV

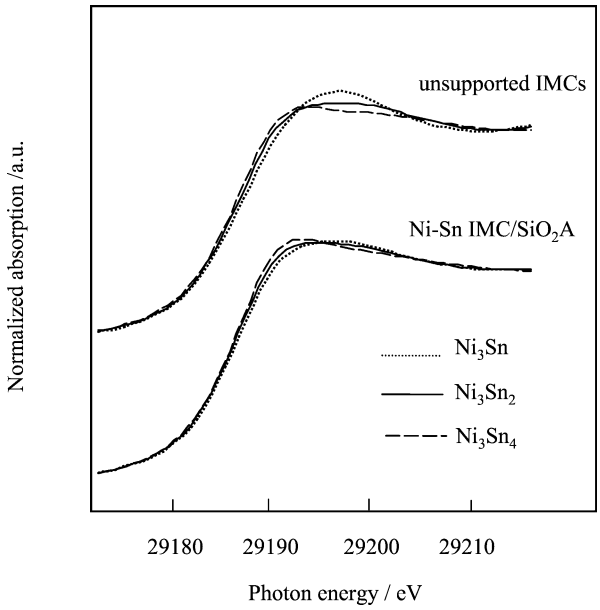

Fig. 7. Sn *K*-edge XANES spectra of unsupported Ni–Sn IMCs and Ni–Sn IMC fine particles supported on SiO_2A.

is the same as those of unsupported series. In conclusion, the prepared Ni–Sn species on SiO_2A are fine particles of the corresponding Ni–Sn IMCs, which can be identified by surface and bulk characterizations of ICP, XPS, TPR, and XANES.

3.2. Catalytic properties for the dehydrogenation of cyclohexane

Dehydrogenation of cyclohexane was carried out over Ni–Sn IMC fine particles supported on SiO_2A. Hydrogen was used as a carrier gas in order to prevent the deactivation of catalysts, especially pure Ni catalyst. This reaction condition was the same as that of our previous work. The results are summarized in Table 3. The products were benzene of the dehydrogenation and methane of the hydrogenolysis. Over Ni/SiO_2A, benzene selectivity was 98% C at 4% of cyclohexane conversion, whereas the selectivity was 2% C at 99% conversion. In contrast, over Ni–Sn IMC/SiO_2A catalysts, benzene selectivity was always higher than 99% C, irrespective of cyclohexane conversion. The high benzene selectivity is related to CO molecule adsorption in only the linear type on Ni–Sn IMC/SiO_2A samples as shown in IR spectra (Fig. 3). The side reaction, i.e., the hydrogenolysis into methane, needs neighboring nickel atoms which made the bridge-type adsorption of CO molecules. As reported previously, the same high selectivity to benzene was observed over Ni–Sn IMC/SiO_2C and unsupported IMC catalysts [15].

As shown in Table 1, the diameters of Ni–Sn IMC particles on SiO_2A were 3–4 nm, which are too large to have a significant size effect on the catalytic properties in the case of Pt and Au catalysts [16–18]. In this study, the selectivity of Ni–Sn IMC fine particle catalysts was also almost the same as that of unsupported Ni–Sn IMC catalysts.

Table 3
Catalytic properties of Ni/SiO_2A and Ni–Sn IMC/SiO_2A catalysts for the reaction of cyclohexane at 673 K for 2 h on stream

Catalyst	Conversion (%)	Benzene selectivity (% C)
Ni/SiO_2A	4	98
	27	83
	99	2
Ni_3Sn/SiO_2A	4	100
	8	100
	56	99
Ni_3Sn_2/SiO_2A	6	100
	11	100
	35	99.5
Ni_3Sn_4/SiO_2A	1.2	100
	3.5	100

Table 4
Activities per weight of nickel and tin metals of supported Ni–Sn IMC catalysts at 2 h on stream for the reaction of cyclohexane at 673 K

Support	Activity per metal (μmol $g^{-1}_{(Ni+Sn)}$ s^{-1})			
	Ni	Ni_3Sn	Ni_3Sn_2	Ni_3Sn_4
SiO_2A	17000	2400	1000	0.9
SiO_2C	2100	160	74	0.03

However, the Ni–Sn IMC fine particles seemed to show a significant improvement in specific catalytic activity. The catalytic activities of Ni–Sn IMC/SiO_2A were compared to those of Ni–Sn IMC/SiO_2C as summarized in Table 4. The amount of catalyst and the feed rate of reactant were varied to control the conversion of cyclohexane to less than 10%. Both SiO_2A and SiO_2C by themselves did not catalyze the reaction. On the same support, the order of activity was as follows,

$$Ni > Ni_3Sn > Ni_3Sn_2 > Ni_3Sn_4.$$

The fine-particle catalysts (Ni–Sn IMC/SiO_2A) exhibited higher activity than Ni–Sn IMC/SiO_2C catalysts. Comparing activities per weight of Ni and Sn metals, the activities of Ni_3Sn, Ni_3Sn_2, and Ni_3Sn_4 on SiO_2A were 15, 13, and 30 times higher than those of the corresponding large particles on SiO_2C, respectively, though the comparison between Ni_3Sn_4 catalysts may not be accurate because of their low conversion. The average diameters of Ni_3Sn, Ni_3Sn_2, and Ni_3Sn_4 on SiO_2C were about 18, 12, and 12 nm, respectively [15]. According to calculations based on the average diameters, specific surface areas of Ni_3Sn, Ni_3Sn_2, and Ni_3Sn_4 on SiO_2A should be about 6, 3.5, and 3 times larger than those on SiO_2C. The increase in activity per weight was significantly larger than that in specific surface area, even though there could be a 50% error in these specific surface areas. The size effect of Ni–Sn IMC fine particles could be the explanation for the improvement in specific activity. The Ni–Sn IMC fine particles with diameter smaller than 3 nm

could show not only further improved specific activity but also different selectivity for particular reactions.

4. Conclusions

Fine-particles of single-phase Ni–Sn IMCs (Ni_3Sn, Ni_3Sn_2, and Ni_3Sn_4) are prepared by the CVD of $Sn(CH_3)_4$ onto fine nickel particles on SiO_2 at optimum temperature and a hydrogen treatment at 773 K. The bulk and surface structures of these particles are very similar to those of corresponding unsupported Ni–Sn IMCs, which is indicated from reduction behaviors revealed by TPR, near-surface Ni/Sn atomic ratios estimated by XPS, and bulk conditions clarified by Ni *K*-edge and Sn *K*-edge XANES measurements.

Carbon monoxide chemisorbs linearly on all Ni–Sn IMC particles. The amount of carbon monoxide chemisorbed on Ni–Sn IMCs supported on SiO_2 is comparable to that chemisorbed on pure nickel supported on SiO_2 and decreases with increasing tin contents. In contrast, hydrogen scarcely chemisorbs on Ni_3Sn_2 and Ni_3Sn_4.

In the catalytic dehydrogenation of cyclohexane, the Ni–Sn IMC fine particles supported on SiO_2 have almost the same selectivity to benzene as the large-particle Ni–Sn IMC catalysts supported on SiO_2 and the unsupported Ni–Sn IMC catalysts. The fine-particle catalysts have a specific activity per weight of Ni and Sn an order of magnitude higher than the large-particle catalysts.

Acknowledgments

The authors thank Dr. S. Takenaka and Prof. K. Otsuka for measurements and analysis of XAFS spectra. The authors thank Prof. S. Namba for measurements of TEM. The X-ray adsorption experiment was performed under the approval of the Photon Factory Program Advisory Committee (Proposal No. 2000G075).

References

[1] W.E. Wallace, Chemtech 12 (1982) 752.
[2] T. Takeshi, W.E. Wallace, R.S. Craig, J. Catal. 44 (1976) 236.
[3] K. Soga, H. Imamura, S. Ikeda, J. Phys. Chem. 81 (1977) 1762.
[4] T.P. Chojnacki, L.D. Schmidt, J. Catal. 129 (1991) 473.
[5] T. Komatsu, M. Fukui, T. Yashima, 11th Intern. Congr. Catal.—40th Anniversary, Stud. Surf. Sci. Catal. 101 (1996) 1095.
[6] T. Komatsu, S. Hyodo, T. Yashima, J. Phys. Chem. B 101 (1997) 5565.
[7] A. Onda, T. Komatsu, T. Yashima, Phys. Chem. Chem. Phys. 2 (2000) 2999.
[8] Asahi Kasei, Japan patent Kokai 10-216515 (1998).
[9] T. Komatsu, D. Satou, A. Onda, Chem. Commun. (2001) 1080.
[10] J.P. Candy, A.E. Mansour, O.A. Ferretti, G. Mablion, J.P. Bournonville, J.M. Basset, G.J. Martino, J. Catal. 112 (1988) 201.
[11] P. Lesage, O. Clause, P. Moral, B. Didillon, J.P. Candy, J.M. Basset, J. Catal. 155 (1995) 238.
[12] K. Tomishige, K. Asakura, Y. Iwasawa, J. Catal. 149 (1994) 70.
[13] G.F. Santri, M.L. Casella, G.J. Siri, H.R. Aduriz, O.A. Ferretti, Appl. Catal. A 197 (2000) 141.
[14] A. Onda, T. Komatsu, T. Yashima, Chem. Commun. (1998) 1507.
[15] A. Onda, T. Komatsu, T. Yashima, J. Catal. 201 (2001) 13.
[16] M. Haruta, S. Tsubota, T. Kobayashi, M. Kageyama, J. Genet, B. Delmon, J. Catal. 114 (1993) 175.
[17] J.C. Frost, Nature 334 (1988) 577.
[18] N. Ichikuni, Y. Iwasawa, Catal. Lett. 20 (1993) 87.
[19] F.W. Lytle, R.B. Greegor, E.C. Marques, V.E. Biebesheimer, D.R. Sandstorm, J.A. Horseley, J.M. Sinfelt, in: M.L. Devieney, J.L. Grand (Eds.), Catalysts Characterization Science, Surface and Solid State Chemistry, Am. Chem. Society, Washington, DC, 1985.
[20] D.C. Koningsberger, R. Prins (Eds.), X-Ray Adsorption: Principles and Applications, Techniques of EXAFS, SEXAFS and XANES, Wiley, New York, 1988.
[21] Y. Iwasawa (Ed.), X-Ray Adsorption Fine Structure for Catalysts and Surface, Series on Synchrotron Radiation, Techniques and Applications, Vol. 2, World Scientific, Singapore, 1996.
[22] T.B. Massalski, H. Okamoto, P.R. Subramanian, L. Kacprzak (Eds.), Binary Alloy Phase Diagrams, second ed., ASM International and National Institute of Standard and Technology, 1990.
[23] M. Nomura, A. Koyama, KEK Rep. 89 16 (1989) 1.
[24] S. Yoshida, S. Takenaka, T. Tanaka, H. Hirano, H. Hayashi, Stud. Surf. Sci. Catal. 101 (1996) 871.
[25] G.E. Moulder, W.F. Stickle, P.E. Sobol, K.D. Bomben (Eds.), Handbook of X-Ray Photoelectron Spectroscopy, second ed., Perkin–Elmer, Physical Electronics Division, 1992.
[26] F.U. Hillebrecht, J.C. Fuggle, P.A. Bannet, Z. Zolnierec, C. Freiburg, Phys. Rev. B 27 (1982) 2179.
[27] W.F. Pong, K.P. Lin, Y.K. Chang, M.H. Tsai, H.H. Hsieh, J.Y. Pieh, P.K. Tseng, J.F. Lee, L.S. Hsu, J. Synchrotron Rad. 6 (1999) 731.
[28] D.T. Jiang, T.K. Sham, P.R. Norton, S.M. Heald, Phys. Rev. B 49 (1994) 3709.
[29] A. Bzowski, T.K. Sham, Phys. Rev. B 48 (1993) 7836.